

Time-dependent electron transport through a strongly correlated quantum dot: multiple-probe open boundary conditions approach

A. Pertsova, M. Stamenova and S. Sanvito

School of Physics and CRANN, Trinity College Dublin, Dublin 2, Ireland

(Dated: December 7, 2018)

We present a time-dependent study of electron transport through a strongly correlated quantum dot. The time-dependent current is obtained with the multiple-probe battery method, while adiabatic lattice density functional theory in the Bethe ansatz local-density approximation to the Hubbard model describes the dot electronic structure. We show that for a certain range of voltages the quantum dot can be driven into a dynamical state characterized by regular current oscillations. This is a manifestation of a recently proposed dynamical picture of Coulomb blockade. Furthermore, we investigate how the various approximations to the electron-electron interaction affect the line-shapes of the Coulomb peaks and the I - V characteristics. We show that the presence of the derivative discontinuity in the approximate exchange-correlation potential leads to significantly different results compared to those obtained at the simpler Hartree level of description. In particular, a negative differential conductance (NDC) in the I - V characteristics is observed at large bias voltages and large Coulomb interaction strengths. We demonstrate that such NDC originates from the combined effect of electron-electron interaction in the dot and the finite bandwidth of the electrodes.

PACS numbers: 05.60.Gg, 71.10.Fd, 73.23.Hk

I. INTRODUCTION

Electron transport through nanoscale devices is a diverse subject, which is currently the focus of extensive experimental and theoretical research. The fuel of such interest is the expectation that nanoscale objects, such as quantum dots¹ and even single molecules,² are to become active components in novel electronic devices, which potentially offer unique advantages over existing technologies.³ At the fundamental level, the physics of such reduced-dimensional systems is dominated by quantum effects. Among them are electron correlations, which strongly affect the electron transport at this level of confinement, giving rise to prototypical quantum phenomena, such as Coulomb blockade^{4,5} and the Kondo effect.⁶⁻⁸

While the Landauer formula is the solution to the non-interacting quantum transport problem,⁹ the interacting case continues to be challenging to the theory. The latter is typically approached with the non-equilibrium Green's function (NEGF) formalism,¹⁰ which allows, in principle, the derivation of an interacting many-body Landauer-type formula for the steady-state current in the case where interaction is limited to a finite region in space.¹¹ In practice, for the majority of the state-of-the-art *ab initio* transport calculations and numerical algorithms,¹²⁻¹⁵ the method of choice for the electronic structure description is the density functional theory (DFT). However, typical steady-state DFT+NEGF transport schemes have a range of limitations, both conceptual and technical.¹⁶

At the fundamental level it has been recently demonstrated, at least for the case of a single Anderson impurity model, that the linear response conductance calculated from the Kohn-Sham levels for the exact exchange-correlation (XC) functional reproduces closely that com-

puted with many-body approaches.^{17,18} If the same holds true for *ab initio* DFT, then the DFT+NEGF scheme will provide a complete solution for the zero-bias limit. Still, on the practical side, the commonly used approximations to the XC functional, lacking the so-important derivative discontinuity,¹⁹ fail to capture essential physics for the transport in molecular junctions, qualitatively mispredicting the conduction regime.^{20,21} Different is the situation at finite bias, where, let alone the implementation, conceptual concerns reflect on the very applicability of a ground-state electronic structure theory to an intrinsically non-equilibrium problem especially if electron correlations are significant.^{22,23}

One strategy to avoid some of the shortcomings of using equilibrium DFT has been sought in its natural extension, time-dependent (TD) DFT,²⁴ with practical schemes for TD transport having been developed.¹⁶ In general, real-time TD schemes for quantum transport can be roughly divided into two categories based on their assumption for the initial conditions. In one case the electrodes are prepared in equilibrium with the poles of a battery, but not yet connected to the nanoscopic device. The current then starts to flow when the connection is made. In the other the system electrodes+device is initially at equilibrium and subsequently an electric field is applied to the electrodes. The former assumption, where two initial electrochemical potentials are well defined, is more in the spirit of the Landauer transport picture. The latter is instead more DFT-friendly, as the starting point is the ground state of the system.¹⁶

There has been evidence that these two TD transport variants agree in the non-interacting case, i.e. they lead to the same history-independent steady-state current.^{25,26} More recently, the latter variant combined with the TDDFT, further equipped with a novel XC functional carrying the physical derivative discontinuity, has been

applied to study the transport through a quantum dot in the Coulomb blockade (CB) regime by Kurth *et al.* in Ref. [27]. In particular that work has put forward an important novel description of CB as a dynamical process with rapidly oscillating local currents, inaccessible by conventional steady-state transport models.

In this work we adopt another recently proposed TD transport scheme, the so-called, *multiple-probe battery* (MPB) method,^{28,29} to study electron transport through a strongly correlated quantum dot. The MPB scheme was first proposed in the context of correlated electron-ion dynamics and was applied to a wide range of problems, such as current-induced heating in atomic wires.^{28,30} This method belongs to the first of the fore-mentioned categories and enables the realization of an external battery within the finite system of electrodes+device. The external bias is introduced through the difference in the electrochemical potentials of the set of reservoirs, or *probes*, attached individually to each atom in a pair of large but finite metallic electrodes (leads). The scheme is very tractable computationally and has the control knobs to be an arbitrarily close approximation to the non-interacting Landauer transport in the long-time dc limit.

The MPB time-propagation scheme is based on the integration of the Liouville-von Neumann equation of motion for the reduced density matrix of the system, in which the open boundaries are described explicitly by a source and a drain term. For the TD Hamiltonian of the quantum dot, entering the equation of motion, we adopt the description used by Kurth *et al.*²⁷ This is based on the adiabatic Bethe ansatz local-density approximation³¹ (adiabatic BALDA, or ABALDA) to the XC functional, which exhibits a derivative discontinuity at half-filling.

By investigating the real-time evolution of the current through the quantum dot, we find an agreement with Ref. [27], i.e. for a certain set of parameters the system does not reach a steady state but rather remains in a dynamical state, characterized by oscillations in the current. Furthermore, we try to interpret the TD results in terms of the more familiar steady-state picture of transport. In particular, we construct the current-voltage, I - V , characteristics of the quantum dot from the long-time average of the current and the voltage obtained from the TD simulations. This is done for a wide range of parameters, even in the cases when a steady state is not achieved. Importantly, we observe a drop of the current as a function of the source-drain voltage and, as a consequence, a negative differential conductance (NDC) above a critical bias voltage. We demonstrate that such an effect is not possible if the derivative-discontinuity is not included in the one-particle potential.

This is particularly interesting in view of some recent contrasting results. On the one hand a number of studies, based on several distinct many-body approaches,³²⁻³⁴ attribute the NDC mainly to electron-electron interaction. On the other hand, it has been demonstrated by Bâldea and Köppel³⁵ that in the case of an exactly solv-

able model for a non-interacting dot within the steady-state formalism, the finite bandwidth of the electrodes can alone lead to pronounced NDC for a wide range of parameters. Here we find a numerical proof that this result can be generalized to the interacting case and time-dependent transport. Our calculations suggest, however, that for the system considered here, the NDC is due to a combination of two effects, namely electron-electron interaction on the dot *and* the finite bandwidth of the electrodes.

Our paper is organized as follows. In the next section we introduce the model system and our theoretical framework, i.e. the Hamiltonian and the computational scheme for MPB quantum transport. In the first part of Section III the I - V characteristics of a non-interacting quantum dot calculated by using the TD-MPB method is compared to analytic NEGF results. We then discuss the finite electrode bandwidth as a source of NDC. In the second part of Section III, we present the TD results for a strongly correlated dot in the CB regime. Finally, we propose an explanation for the observed NDC in the I - V characteristics.

II. METHODS

The model system considered in this work is presented in Fig. 1. This consists of a central region, which contains the quantum dot surrounded by two N_d -site long atomic chains at both sides, and two one-dimensional finite leads, each counting $N_{L(R)}$ atoms. The physics of the quantum dot connected to two leads is described by the Anderson impurity model.^{11,36} The Hamiltonian of the total system thus reads

$$\hat{H}_S = \sum_{\alpha=L,R} \hat{H}_\alpha + \hat{H}_T + \hat{H}_{\text{QD}}. \quad (1)$$

Here the first term is the nearest-neighbors single-orbital tight-binding (TB) Hamiltonian describing respectively the left-hand side ($\alpha=L$) and right-hand side ($\alpha=R$) lead. This is written as

$$\hat{H}_\alpha = \sum_{i,\sigma} \varepsilon_{i\alpha} \hat{c}_{i\alpha}^{\sigma\dagger} \hat{c}_{i\alpha}^\sigma + \sum_{i,\sigma} \gamma_0 \left(\hat{c}_{i\alpha}^{\sigma\dagger} \hat{c}_{i+1\alpha}^\sigma + h.c. \right), \quad (2)$$

where $\varepsilon_{i\alpha}$ are the on-site energies and γ_0 is the hopping integral; $\hat{c}_{i\alpha}^{\sigma\dagger}(\hat{c}_{i\alpha}^\sigma)$ is the creation (annihilation) operator for an electron with spin σ ($\sigma=\uparrow, \downarrow$) at the atomic site i of the lead α (the index $i = 1, \dots, N_\alpha$ runs from left to right for $\alpha=R$ and from right to left for $\alpha=L$). Note that two atomic chains on each side of the quantum dot are also described by a TB model with the hopping integral γ_0 and therefore they are included in the Hamiltonian of the leads.

The second term in Eq. (1) describes the tunneling between the quantum dot and the two adjacent sites and it is given by

$$\hat{H}_T = \sum_{\sigma} \gamma_c \left(\hat{c}_0^{\sigma\dagger} \hat{c}_{1L}^\sigma + \hat{c}_0^{\sigma\dagger} \hat{c}_{1R}^\sigma + h.c. \right), \quad (3)$$

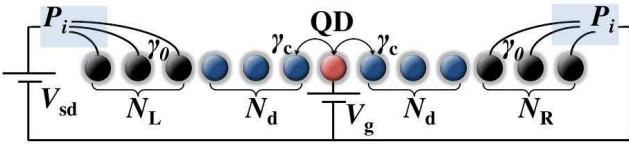


FIG. 1: (Color online) Schematic of the model system considered in this work: the central region consists of a quantum dot (QD) surrounded by two N_d -site long atomic leads, which in turns are attached to two one-dimensional leads comprising respectively N_L and N_R sites. Here γ_0 is the hopping integral in the leads and in the two chains, and γ_c is the lead to dot hopping. V_g denotes the gate voltage, acting locally on the dot, and V_{sd} is the source-drain voltage applied across the entire system.

where $\hat{c}_0^{\sigma\dagger}$ (\hat{c}_0^σ) is the creation (annihilation) operator for an electron with spin σ on the dot and γ_c is the hopping integral between the dot and site $i=1$ in the lead α .

Finally, the Hamiltonian of the quantum dot reads

$$\hat{H}_{\text{QD}} = \sum_{\sigma} V_g \hat{n}_0^{\sigma} + U \hat{n}_0^{\uparrow} \hat{n}_0^{\downarrow}, \quad (4)$$

where V_g is the on-site energy of the dot, which acts as a local gate voltage; U ($U \geq 0$) is the charging energy, which expresses the strength of the Coulomb repulsion on the dot; $\hat{n}_0^{\sigma} = \hat{c}_0^{\sigma\dagger} \hat{c}_0^{\sigma}$ is the site-occupation operator.

Within the lattice DFT framework³⁷ the many-body Hamiltonian in Eq. (4) is mapped onto an effective single-particle Kohn-Sham Hamiltonian which, in the local density approximation, reads

$$\hat{H}_0 = \sum_{\sigma} v_{\text{KS}}[n_0] \hat{n}_0^{\sigma}. \quad (5)$$

Here n_0 is the charge density of the dot and v_{KS} is the effective Kohn-Sham potential, which can be written as a sum of three terms

$$v_{\text{KS}}[n_0] = V_g + \frac{n_0}{2}U + v_{\text{XC}}[n_0]. \quad (6)$$

The second and third terms are respectively the Hartree and the XC potential. The latter is approximated by a modified BALDA potential, specifically tailored to a nonuniform configuration with a weakly coupled dot (we refer to Ref. [27] for the exact expression and the parametrization).

Notably, such v_{XC} exhibits a derivative discontinuity at $n_0=1$, i.e. at the phase transition of the 1D Hubbard model. In practice, however, we use a continuous approximation to the BALDA potential²⁷ where the true discontinuity, expressed through a Heaviside step function $\theta(n_0)$, is replaced by a function $f(n_0) = 1/(e^{(n_0-1)/a} + 1)$ with a being a smoothing parameter. We use $a = 10^{-7}$, which guarantees a very sharp slope at $n_0 = 1$. In our simulations we consider three levels of description: (i) $U = 0$, or non-interacting case, for which the effective potential of the dot is simply given by $v_{\text{KS}}=V_g$, (ii)

$v_{\text{XC}} \rightarrow 0$, or the Hartree approximation, where the potential on the dot is $v_{\text{H}}=V_g + U n_0/2$; and (iii) the full discontinuous effective potential, given by Eq. (6), which we refer to as v_{KS} for clarity.

In order to introduce the time-dependence in the Hamiltonian of the quantum dot, we use the adiabatic approximation, where v_0 is assumed to depend on time only through the instantaneous charge density of the dot

$$v_{\text{KS}}(t) = v_{\text{KS}}[n_0(t)]. \quad (7)$$

The question of the applicability of such adiabatic local approximation to the description of non-equilibrium transport in strongly correlated systems has been addressed in recent two works respectively by Uimonen *et al.*³⁸ and Khorsavi *et al.*³⁹ In particular, a comparative study between the TDDFT approach with ABALDA (TDDFT+ABALDA) and the many-body perturbation theory, applied to out-of-equilibrium Anderson impurity model, has been carried out in Ref. [38]. The results obtained with both approaches have been tested against numerically exact results produced by time-dependent density matrix renormalization group theory. It was found that, in general, the TDDFT+ABALDA approach is in good qualitative agreement with many-body perturbation theory over a wide range of parameters. However, in many cases it overestimates the steady-state currents. This problem was linked to the shortcomings of the local approximation to the XC functional and, in particular, to the absence of electron correlations inside the electrodes. Moreover, it was demonstrated in Ref. [39] that the inclusion of dynamical correlations, or memory effects, might eliminate the multistability in the density and the current, which can be found within the TDDFT+ABALDA approach. These are strong indications that more advanced non-local, both in space and time, approximations to the XC functional are required. However, as was demonstrated in Ref. [27] and as it will be shown in this paper, the ABALDA already provides valuable insights into time-dependent transport in strongly correlated systems.

We now discuss, following the work of Todorov and co-workers,^{28,29} how the open boundary conditions are introduced in the MPB setup. In the MPB method, each atom i of the leads (with the exception of the N_d atoms at both sides of the quantum dot) is connected to an external probe P_i (see Fig. 1). All the probes attached to the sites in the left (right) lead are kept at the electrochemical potential μ_L (μ_R) and are occupied according to the Fermi-Dirac distribution f_L (f_R). The source-drain voltage V_{sd} is introduced as $V_{sd} = \mu_L - \mu_R$ (here V_{sd} is in units of eV). For symmetrically applied bias $\mu_L = \varepsilon_F + V_{sd}/2$ and $\mu_R = \varepsilon_F - V_{sd}/2$, where ε_F is the Fermi level of the electrodes (assumed identical). The time-dependent equation of motion for the density matrix of the system

coupled to the probes reads

$$i\hbar \dot{\hat{\rho}}_S(t) = \left[\hat{H}_S(t), \hat{\rho}_S(t) \right] + \hat{\Sigma}^+ \hat{\rho}_S(t) - \hat{\rho}_S(t) \hat{\Sigma}^- + \quad (8) \\ + \int_{-\infty}^{\infty} \left[\hat{\Sigma}^<(E) \hat{G}_S^-(E) - \hat{G}_S^+(E) \hat{\Sigma}^<(E) \right] dE.$$

The last two terms on the right-hand side are extraction (drain) and injection (source) terms, respectively; \hat{G}^+ (\hat{G}^-) is the retarded (advanced) Green's function of the system and it is given by

$$\hat{G}^\pm = \left(E \hat{I}_S - \hat{H}_{S_0} - \hat{\Sigma}^\pm \pm i \hat{I}_S \Delta \right)^{-1}, \quad (9)$$

where $\hat{H}_{S_0} = \sum_{\alpha=L,R} \hat{H}_\alpha + \hat{H}_T + \sum_\sigma V_g \hat{n}_0^\sigma$ is the time-independent part of $\hat{H}_S(t)$ and Δ is a dephasing factor (see later for an exact definition). The self-energies due to the presence of the external probes and the in-scattering self-energy are written as

$$\hat{\Sigma}^\pm = \mp i \frac{\Gamma}{2} \hat{I}_L \mp i \frac{\Gamma}{2} \hat{I}_R, \quad (10)$$

$$\hat{\Sigma}^< = \frac{\Gamma}{2\pi} f_L(E) \hat{I}_L + \frac{\Gamma}{2\pi} f_R(E) \hat{I}_R, \quad (11)$$

with the broadening Γ defined as $\Gamma = 2\pi\gamma_P^2 d$, where γ_P is the coupling to the probes, assumed to be identical for all sites in the leads, and d is an energy-independent constant, which represents the surface density of states of the probes within the wide-band limit; \hat{I}_M is the identity operator in region M (M=L, R, S).

Equation (8) is derived from a general Liouville-von Neumann equation for the total density matrix of the system and the probes combined. It incorporates two main approximations: (i) the wide-band limit in the probes and (ii) the decoherence in the injection process, introduced through the relaxation time τ_Δ , with $\Delta = \hbar/\tau_\Delta$ [see Eq. (9)]. The second approximation essentially decouples, over the time interval τ_Δ , the injection of electrons from the probes into the leads and their subsequent scattering from the time-dependent potential inside the central region, provided that the latter is long enough. In other words the dephasing factor imposes a restriction on the size of the central region ($2N_d + 1$ sites). Therefore the inclusion of N_d buffer sites on both sides of the dot is essential within the time-dependent formalism.

The value of Δ is determined in such way that the distance traveled by the electrons during the time interval τ_Δ is smaller than the distance between the electrodes and the interior of the central region, i.e. the quantum dot. This condition can be written as $v_e \tau_\Delta < N_d a$, where v_e is the electron group velocity and a the lattice constant ($a = 1$). In practical terms, the introduction of the dephasing factor allows one to write down the injection term, which is in general non-local in time, in a rather simple time-independent form [see Eq. (8)]. This, however, also introduces an additional broadening, proportional to Δ , in the steady-state I - V characteristics,

which is absent in the standard static NEGF formalism. We note that in the steady-state MPB formalism, the NEGF result is recovered in the limit of infinitely long leads and weak lead-probe coupling.²⁹

In order to investigate the open-boundary electron dynamics in the time domain, Eq. (8) is numerically-integrated using the fourth-order Runge-Kutta (RK4) algorithm.⁴⁰ As initial condition, we use the density matrix $\hat{\rho}_S(t_0)$ of an isolated system (not coupled to the probes), constructed from the eigenstates of the Hamiltonian \hat{H}_S . The open boundary terms are switched on over a short time interval of 5 fs and maintained throughout the simulation. The current through the dot is then calculated as a bond current between the dot and the adjacent site.⁴¹ The typical parameters of the MPB setup used in our simulations, unless specified otherwise, are $N_{L/R} = 90$ and $N_d = 20$. We have tested that further increasing the size of the system does not lead to significant difference in the I - V characteristics. In order to have one free parameter instead of two, we use the condition $\Delta = \Gamma/2$, which has been discussed in detail in Ref. [28], and $\Gamma = 0.35$ eV in our simulations.

III. RESULTS

A. Non-interacting case

As a test of the applicability of the TD MPB method we first examine the non-interacting case ($U = 0$). For this situation, we directly compare the I - V characteristics obtained from the time-dependent simulations to the ones calculated by using the standard NEGF-based Landauer solution, which we refer to as exact NEGF.¹⁰ The comparison is presented in Fig. 2, where the current is plotted as a function of the source-drain voltage for the non-interacting level aligned with the Fermi level in the leads ($V_g = 0$). In the case of the TD MPB approach, the value for the steady-state current is obtained from the time-dependent simulation for the corresponding value of V_{sd} after the steady-state has been established, i.e. when the variation of the current with time becomes negligible. In the case of the exact NEGF method, we use the well-known analytical expression for the non-equilibrium current through a non-interacting resonant level coupled to two semi-infinite electrodes^{10,35}

$$I_{EN} = \frac{2e}{h} \int dE \frac{\Gamma_L(E) \Gamma_R(E)}{[E - V_g - \Lambda(E)]^2 + [\Gamma(E)/2]^2} \times \\ \times [f_L(E) - f_R(E)]. \quad (12)$$

Here $\Lambda(E) = \Lambda_L(E) + \Lambda_R(E)$ and $\Gamma(E) = \Gamma_L(E) + \Gamma_R(E)$ represent, respectively, the real and imaginary part of the total self-energy due to the presence of electrodes, with

$\Lambda_{L(R)}$ and $\Gamma_{L(R)}$ given by

$$\Lambda_{L(R)}(E) = \frac{\gamma_c^2}{2\gamma_0^2} E_{L(R)}, \quad (13)$$

$$\Gamma_{L(R)}(E) = \frac{\gamma_c^2}{\gamma_0^2} \theta(2\gamma_0 - |E_{L(R)}|) \sqrt{4\gamma_0^2 - E_{L(R)}^2}, \quad (14)$$

where $E_\alpha \equiv E - \varepsilon_\alpha$, ε_α being the on-site energy in the lead ($\alpha = L, R$).

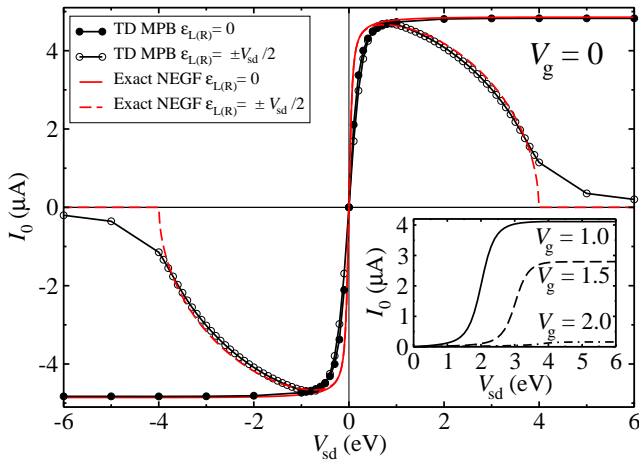


FIG. 2: (Color online) Current through the quantum dot, I_0 , as a function of the source-drain voltage, V_{sd} , for zero gate voltage ($V_g=0$), calculated using the both exact NEGF and the TD MPB method, and for two configurations of the leads: $\varepsilon_{L/R}=0$ and $\varepsilon_{L/R}=\pm V_{sd}/2$. The inset shows the I - V characteristics obtained with the TD MPB approach for $\varepsilon_{L/R}=0$ and three different gate voltages, $V_g=1.0, 1.5$ and 2.0 eV. The following parameters are used: $\gamma_0=-1.0$ eV, $\gamma_c=-0.1$ eV and $\varepsilon_F=0$. The source-drain voltage is applied symmetrically, $\mu_{L/R}=\varepsilon_F \pm V_{sd}/2$. In order to achieve a better agreement with the exact NEGF results we use the improved MPB setup with $N_{L(R)} = 250$, $N_d = 90$ and $\Gamma = 0.15$.

We consider two possible limits for the on-site energies in the electrodes: (i) the highly conducting regime with $\varepsilon_\alpha=0$ for all atoms in $\alpha = L, R$ and (ii) the weakly conducting regime for which the on-site energies in L(R) are shifted in accordance with the respective electrochemical potential, $\varepsilon_{L(R)}=\pm V_{sd}/2$. As expected, the difference between the I - V curves calculated in these two limits becomes significant at large bias, since the transmission in case (ii) rapidly drops to zero once the bias voltage exceeds the bandwidth of the leads ($4|\gamma_0|$). This high-bias NDC effect, stemming entirely from the finite electrode band-width, is a well-understood feature of steady-state transport in low-dimensional yet uncorrelated electron systems.³⁵ We also note that the low-bias agreement between the two transport limits can, in principle, be extended to arbitrarily high biases V_{sd} by increasing $\gamma_0 > V_{sd}/4$.⁴⁵

An encouraging result is that for both the transport limits the TD MPB method reconstructs rather well the

exact NEGF I - V . The agreement is particularly good in the highly conducting limit. The smearing of the abrupt I - V features at low bias and again the NDC drop at $V_{sd} \lesssim 4\gamma_0$ for the weakly conducting limit are inherent to the TD MPB method.²⁸ These are due to the explicit dephasing factor, which simplifies the equation of motion for the density matrix by eliminating temporal non-localities of the injection.

In order to eliminate the drop in the current at large bias voltages and to focus on the electron interaction at the quantum dot, we will use the $\varepsilon_{L(R)}=0$ limit in all the further calculations presented. In this case, the saturation current at high voltages is entirely determined by the position of the resonant level, set by the gate voltage V_g (see the inset of Fig 2), relatively to the electrodes band center. As the resonant level approaches the band-edge of the leads ($V_g \lesssim 2\gamma_0$), the saturation current decreases. In Section III B 2 we will recognize the contribution of the latter effect to the drop in the current as a function of the source-drain voltage.

B. Interacting case

1. Time-dependent transport

While in the non-interacting case the TD current through the dot always reaches the steady-state, in the case when electron-electron interaction is considered this is not guaranteed. In fact for certain values of the source-drain voltage, for which the charge density of the dot approaches unity, the system is driven into a dynamical state, where current, density and on-site potential oscillate²⁷ without ever reaching a steady-state.

The question we address here is whether such dynamical state can be captured by the MPB method. The results of our calculations are shown in Fig. 3. For all values of the source-drain voltage below a critical value V_{sd}^{cr} a steady-state is achieved. However, for source-drain voltages above V_{sd}^{cr} , oscillations indeed develop in all transport-related quantities. As shown in Fig. 3 for this range of V_{sd} the density quickly reaches a critical value of $n_0 = 1$. At the same time the first jump of the on-site potential occurs, followed by a series of almost rectangular pulses [see Fig. 3(b)]. Due to the derivative discontinuity at $n_0 = 1$, the on-site potential reaches an oscillating regime, abruptly alternating in time between two values, one just below and the other just above the discontinuity. This translates into oscillations of the charge density around $n_0 = 1$ [see the inset in see Fig. 3(a)] and also into oscillations in the current [Fig. 3(b)].

Below, we elaborate on the dynamical features observed for different values of V_{sd} . The height of the pulses in $v_{KS}(t)$ is equal to the height of the jump of $v_{KS}[n_0]$ at the derivative discontinuity and it is mainly governed by the value of the charging energy U . The width of the pulses increases with increasing V_{sd} . This essentially means that for larger V_{sd} the system tends to stay longer

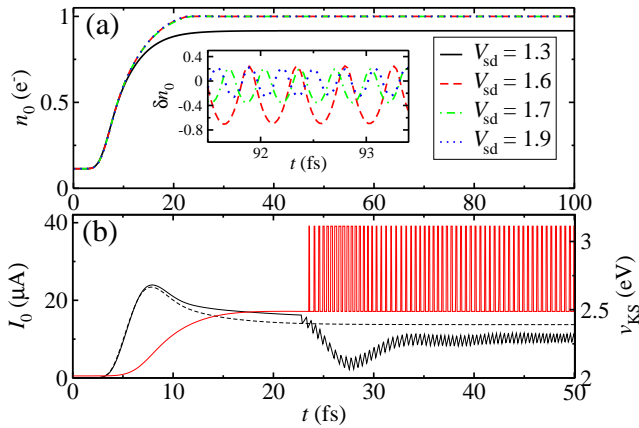


FIG. 3: (Color online) Real-time evolution of the quantum dot: (a) Charge density of the dot (n_0) for four different values of the source-drain voltage, $V_{sd}=1.3, 1.6, 1.7,$ and 1.9 eV. The inset shows the fluctuation of the density around unity, δn_0 , defined as $\delta n_0 = (n_0 - 1) \times 10^3$. (b) Current through the dot, I_0 , for two values of V_{sd} : $V_{sd}=1.6$ eV (black solid line), which corresponds to the oscillating regime, and $V_{sd}=1.3$ eV (black dashed line) where no oscillations are observed. Note that the corresponding Kohn-Sham potential (v_{KS}) [red solid line] is also in the oscillating regime ($V_{sd}=1.6$ eV). The following parameters are used: $\gamma_0=-1.5$ eV, $\gamma_c=-0.3$ eV, $\varepsilon_F=1.5$ eV, $U=2.0$ eV, $\varepsilon_{L(R)}=0$ is taken as a reference of energy. The source-drain voltage is applied asymmetrically ($\mu_L=\varepsilon_F + V_{sd}$, $\mu_R=\varepsilon_F$).

in the state with a larger on-site potential, corresponding to the density above 1. Further increasing V_{sd} will finally lead to a steady-state. The exact value of the threshold voltage, V_{sd}^{cr} , is difficult to determine since the on-site potential changes with time. From simple considerations, however, we established that $V_{sd}^{cr} \geq v_{KS}[\bar{n}]$, where \bar{n} is a value of the charge density just below 1. For the set of parameters used here $V_{sd}^{cr} \approx 1.5$ eV.

As discussed by Kurth *et al.*, the dynamical state of the quantum dot described above is a manifestation of dynamical Coulomb blockade. By applying a large enough source-drain voltage the dot can be charged. However, when the charge reaches the critical value $n_0 = 1$, the on-site potential immediately increases by an amount, determined by Coulomb repulsion U , thus preventing further charging. This essentially corresponds to the CB regime. In addition, the time-dependent simulations reveal that in this regime the quantum dot is alternating between two states, separated by an energy barrier determined by U . These two states correspond to the fluctuation of the charge on the dot around $n_0 = 1$, which originates from the fact that the ABALDA potential has a derivative discontinuity at $n_0 = 1$ but it is a smoothly varying function of n_0 away from this occupation.

It follows from the discussion that the dynamics of the quantum dot in the CB regime, calculated with the TD MPB method, is in a good agreement with the results reported in Ref. [27] both qualitatively and quantitatively.

We have established numerically that the two different methods reproduce practically identical dynamical trajectories for all the observables in the long-time limit in the case of an interacting system. The remaining differences are limited to the early stage of the time-evolution. A characteristic feature of the on-site potential of the dot, observed in Ref. [27], is a transition period just after the start of the oscillations, where the series of rectangular pulses in the time-dependent v_{KS} is preceded by a larger pulse whose width increases with V_{sd} . This characteristic transient pulse is not present in our calculations (see Fig. 3).

In order to establish to what extent the transient pulse is determined by the initial conditions, we performed TD simulations for the same system as shown in Fig. 1 but without attaching the external probes, i.e. for a closed-boundary finite system. Instead, we applied the source-drain voltage as a rigid shift of the on-site energies in the left lead, i.e. a term $V_{sd} \sum_{i,\sigma} \hat{c}_{i\alpha}^{\sigma\dagger} \hat{c}_{i\alpha}^{\sigma}$ has been added to the Hamiltonian \hat{H}_α for $\alpha = L$ [see Eq. (2)] at the start of the TD simulation. We used longer leads ($N_{L/R}=220$) and limited the time of the simulations to 100 fs, which is sufficient to observe the time propagation before the reflections from the finite boundaries start to affect the dynamics. The time-dependence of the charge density, current and on-site potential, obtained from the closed-boundary simulation, is presented in Fig. 4. In contrast to our open-boundary simulations, we indeed observed qualitatively the same transient regime as in Ref. [27]. This is mainly characterized by an earlier onset of the CB oscillations for larger source-drain voltages and by the increase of the width of the first pulse in the time-dependence of the Kohn-Sham potential with increasing V_{sd} .

2. Steady-state transport

In the previous section we demonstrated that, within a certain range of parameters, the derivative discontinuity prevents the quantum dot to evolve towards the steady-state. Outside this range, however, a steady-state is achievable. Here we determine the steady-state current through the dot for various gate voltages and map out the corresponding I - V curves. For situations, where the dot is trapped in oscillations, we take as steady-state current its time-average in the long-time limit.

The linear response conductance as a function of V_g is depicted in Fig. 5. This is calculated as the finite-difference ratio $\Delta I_0 / \Delta V_{sd}$ close to zero bias (for a very low but finite bias $\Delta V_{sd} = 0.01$ eV) and represents an approximation to the zero-bias differential conductance. In the non-interacting case, the conductance is composed of a single peak centered around $V_g=1.5$ eV, which corresponds to the Fermi level of the leads. This is expected from the steady-state picture of transport through a non-interacting resonant level. In principle the width of the resonance peak is given by the dot-lead hopping integral

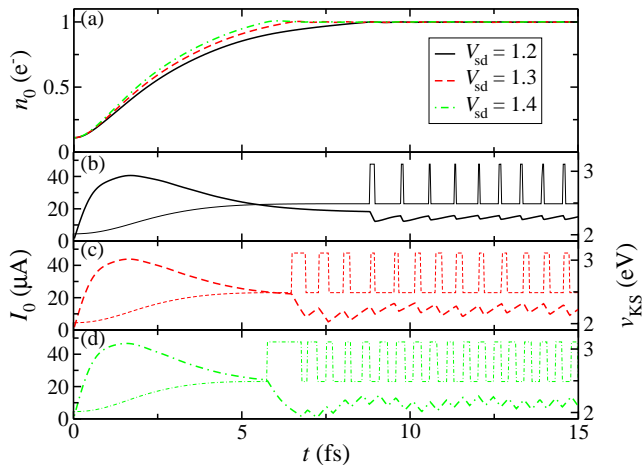


FIG. 4: (Color online) Real-time evolution of the quantum dot in the closed-boundary setup: (a) Charge density of the dot (n_0) for three different values of the source-drain voltage, $V_{sd}=1.2, 1.3,$ and 1.4 eV. Current through the dot, I_0 , [thick lines] and the corresponding Kohn-Sham potential, v_{KS} , [thin lines] for (b) $V_{sd}=1.2$ eV, (c) $V_{sd}=1.3$ eV, and (d) $V_{sd}=1.4$ eV. The parameters are the same as in Fig. 3. The source-drain voltage is applied as a rigid shift of the on-site energies in the left lead.

γ_c . In our TD MPB calculations, however, there is an additional resonance broadening factor (τ_Δ) related to the dephasing condition in the equations of motion. Its corresponding energy unit, $\Delta = \hbar/\tau_\Delta$, can be associated to a fictitious temperature, smearing the electronic energy distributions in the leads.²⁸ As a result, a suppression of the transmission resonance proportional to $1/\Delta$ is also expected. This is the reason of why the amplitude of non-interacting resonance conductance in Fig. 5 is below one quantum of conductance, $G_0 = 2e^2/h$.

In the interacting case the Anderson impurity model predicts two distinct Coulomb peaks⁴² in the conductance as a function of the gate voltage⁴³. These are manifestation of charge quantization at the dot and correspond to each of the two integer electron number states, in which the dot is inhabited by one or two electrons, respectively. Although the ABALDA potential succeeds in describing some important properties of strongly correlated systems,⁴⁴ due to the presence of the derivative discontinuity, it is a single-particle potential and, as such, cannot describe fully these charge states. As a result, the gate-voltage dependence of the conductance, calculated using the full discontinuous effective potential (v_{KS}), does not show two distinct peaks. However, it presents a structure, bearing the signature of two broadened and overlapping peaks (see Fig. 5). The distance between these quasi-peaks increases with increasing U and corresponds to the value of the jump of the on-site potential $v_{KS}[n_0]$ at the derivative discontinuity. In the case of the Hartree approximation, the two-peak structure is less pronounced and the two resonances merge into an

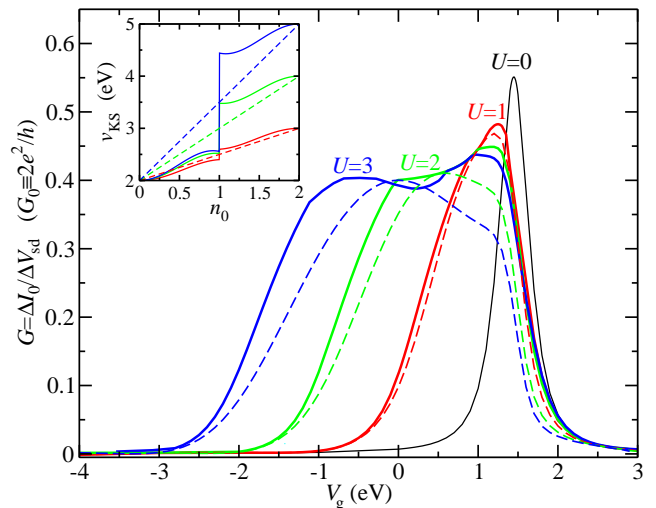


FIG. 5: (Color online) Differential conductance of the dot as a function of the gate voltage (V_g) for the Kohn-Sham potential, v_{KS} , [thick solid lines] and for the Hartree potential, v_H , [dashed lines] with $U=1, 2,$ and 3 eV, and for the non-interacting case (thin solid line). The inset shows a comparison between the density-dependence of v_{KS} (solid lines) and v_H (dashed lines) for the same values of U . Parameters are the same as those of Fig. 3 and $V_{sd} = 0.01$ eV.

asymmetric plateau. The width of this plateau is also proportional to U .

It should be mentioned that for the TD calculations with v_{KS} and for values of V_g between the position of the $U = 0$ resonance level $V_{res} \equiv \varepsilon_F$ and $V_{res} - U$ (roughly corresponding to the region between the two quasi-peaks) no steady-state is achieved. Hence, the conductance curves in this region of V_g carry some degree of arbitrariness, associated with the interpretation of the average TD current. In fact, for those gate voltages driving a charge density at the dot close to unity, even the calculation of the ground-state is problematic from a numerical viewpoint, because of the derivative discontinuity. In such cases we used the following iterative procedure. Let V_g^0 be the value of the gate voltage, for which the ground-state (initial) density is calculated self-consistently, while $V_g^0 + \delta V_g$ is the value of the gate voltage for which the self-consistent calculation does not converge. In this case, the final density, obtained at the end of the time-dependent simulation with $V_g = V_g^0$, is taken as initial density for the simulation with $V_g = V_g^0 + \delta V_g$.

In the same way, from the time-averages in the long time-limit, we map out the I - V characteristics of the interacting dot (v_{KS}) at a given V_g (see Fig. 6). A remarkable feature of the I - V curves is the drop of the current (NDC) at large source-drain voltages, which is almost negligible for small U but increases with increasing U .

For all values of U the current initially increases with increasing V_{sd} as the dot is charging. It then reaches its maximum value as the charge density approaches $n_0 =$

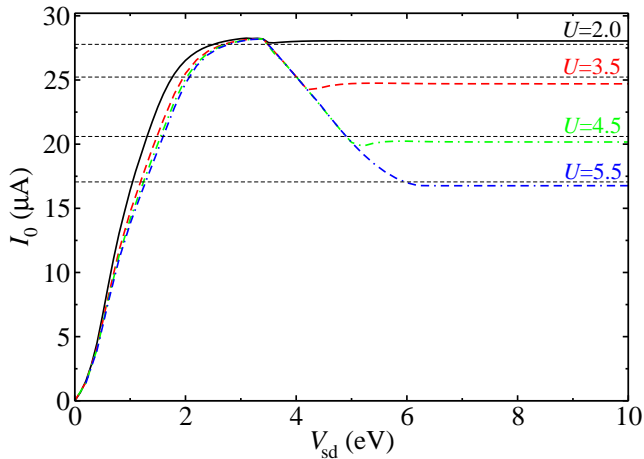


FIG. 6: (Color online) Current through the dot, I_0 , as a function of the source-drain voltage, V_{sd} , for v_{KS} and different values of U . The horizontal dashed lines represent the corresponding saturation currents I_S (see text for the exact definition). The following parameters are used: $\gamma_0 = -3.88$ eV, $\gamma_c = -0.5$ eV, $\epsilon_F = 1.5$ eV, $V_g = 2.0$ eV.

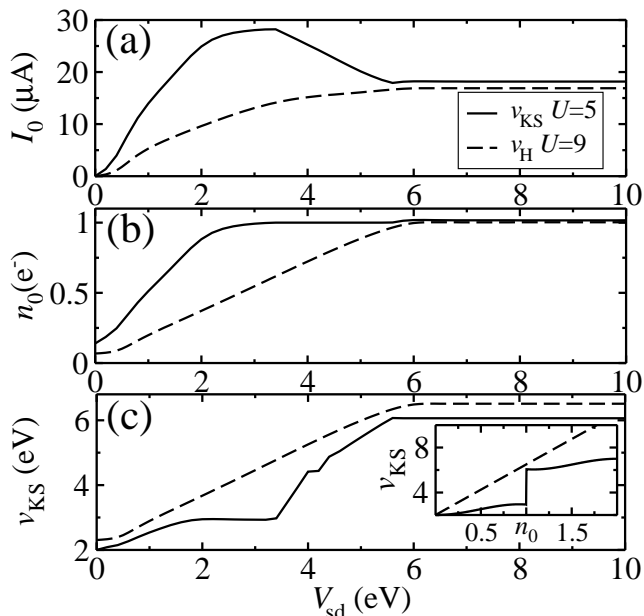


FIG. 7: Current (a), density (b) and on-site potential (c) of the dot as a function of the source-drain voltage, V_{sd} , for v_{KS} with $U = 5$ eV and for v_H with $U = 9$ eV. The inset shows v_{KS} and v_H as functions of the dot density for the corresponding values of U . The parameters are the same as those in Fig. 6.

1. This point corresponds to a threshold source-drain voltage V_{sd}^{cr} , which is roughly the same for all values of U . Beyond V_{sd}^{cr} , the system is driven into a dynamical state (where the steady-state current is calculated by averaging out the oscillations). In the limit of very large V_{sd} , the dot recovers its long-time tendency to a steady state and

the average current saturates. At saturation and beyond the dot occupation is above 1 and the on-site potential assumes a value above the discontinuity. Hence, the on-site energy at the dot is proportional to the the jump of the v_{KS} at $n_0 = 1$, i.e. it is proportional to U .

As discussed in Section III A for the non-interacting case, the saturation current decreases with increasing the dot on-site potential, because of the finite bandwidth of the electrodes. For the same reason here the drop of the current becomes larger when U increases. In fact a large U corresponds to a large value of the steady-state on-site potential, which then approaches the electrodes' band-edge. In order to confirm this conjecture, we compare the saturation current I_S calculated at finite U , with that for $U=0$ and V_g equal to the steady-state on-site potential corresponding to that obtained at the same U . Indeed I_S matches quite well the value of the current obtained at large source-drain voltages in the I - V characteristics of the interacting dot (see horizontal dashed lines next to each curve in Fig. 6). This argument can obviously be reversed, i.e. the NDC cannot be observed, if the variation of the on-site potential at the derivative discontinuity, determined by U , is much smaller than the electrodes' bandwidth. For instance, for the same set of parameters used before for the dot+electrodes system, such NDC-free situation is found for $U = 2$ eV ($U \ll 4|\gamma_0|$ for $\gamma_0 = 3.88$ eV). In this case the drop of the current above V_{sd}^{cr} is practically negligible.

Importantly, the NDC displayed in Fig. 6 is not found in I - V 's calculated within the Hartree approximation, even for large values of U (see Fig. 7). When comparing calculations at the Hartree level with those performed with the complete Kohn-Sham potential we intentionally use different U . These are selected in such a way that the value of the potential at $n_0 = 1$ is identical in the two calculations [see the inset in Fig. 7(c)], i.e. in such a way that the two calculations give the same saturation current. At variance with the complete Kohn-Sham case, in the Hartree only problem the current, as well as the density and the on-site potential, monotonically increase with V_{sd} until the saturation is reached. Based on these numerical results we can argue that the self-interaction-free shape of the on-site potential v_{KS} at the dot is a necessary condition for the occurrence of the NDC in the I - V . The shallow increase of the on-site potential with the charging, produced by the opening of the bias window, keeps the resonant level away from the electrodes band edge and allows the current to rise. Once the on-site charge exceeds $n_0 = 1$ and the resonant level energy shoots up towards the band-edge, the currents drops. The averaged dynamical current monotonically approaches its saturation value corresponding to a steady-state solution.

IV. CONCLUSIONS

We have investigated the electronic transport through a strongly-correlated quantum dot by using a recently proposed multiple-probe battery method for time-dependent simulations of open systems. Our aim was two-fold. Firstly, we wanted to assess the outcomes of a TD transport scheme conceptually different from what used so far in literature, for a problem involving strong electron correlation as in Coulomb blockade. Clearly our MPB-based simulations agree well with previous findings.²⁷ In particular we have demonstrated self-sustained oscillations in the current, density and effective on-site potential, originating from the derivative discontinuity of the approximate exchange-correlation potential used.

As a further aspect we have addressed the question of whether the peculiar dynamics obtained from the time-dependent simulations can be related to the more accessible steady-state picture of transport. In particular, we have shown the presence of Coulomb peaks in the linear response differential conductance and extracted the TD

version of I - V characteristics, based on the time-averaged current through the dot in the long-time limit. The resulting I - V curves, at a critical voltage, exhibit a drop in the average current through the dot. This drop corresponds to the range of parameters where no steady state is found and the dot is in the oscillatory Coulomb blockade state. Such an NDC is however present only when the calculation is performed at a DFT level in which the potential includes the derivative discontinuity at unitary occupation.

Acknowledgments

We are grateful to A. Hurley and I. Rungger for careful reading of the manuscript. We thank T. N. Todorov for very helpful discussions. This work is sponsored by Science Foundation of Ireland (Grant No. 07/IN.1/I945). Computational resources have been provided by the Trinity Center for High Performance Computing.

-
- ¹ R. C. Ashoori, *Nature (London)* **379**, 413 (1996).
² A. Nitzan and M. A. Ratner, *Science* **300**, 1384 (2003).
³ J. C. Cuevas and E. Scheer, *Molecular Electronics: An Introduction to Theory and Experiment* (World Scientific, 2010).
⁴ C. Livermore, C. H. Crouch, R. M. Westervelt, K. L. Campman, A. C. Gossard, *Science* **274**, 1332 (1996).
⁵ J. Park, A. N. Pasupathy, J. I. Goldsmith, C. Chang, Y. Yaish, J. R. Petta, M. Rinkoski, J. P. Sethna, H. D. Abruña, P. L. McEuen and D. C. Ralph, *Nature (London)* **417**, 722 (2002).
⁶ D. Goldhaber-Gordon, H. Shtrikman, D. Mahalu, D. Abusch-Magder, U. Meirav and M. A. Katner, *Nature (London)* **391**, 156 (1998).
⁷ S. M. Cronenwett, T. H. Oosterkamp and L. P. Kouwenhoven, *Science* **281**, 540 (1998).
⁸ W. Liang, M. P. Shores, M. Bockrath, J. R. Long, H. Park, *Nature (London)* **417**, 6890 (2002).
⁹ R. Landauer, *Phil. Mag.* **21**, 863 (1970).
¹⁰ H. Haug and A.-P. Jauho, *Quantum Kinetics in Transport and Optics of Semiconductors* (Springer-Verlag, Berlin, 2008), pp. 59–91, 157–170.
¹¹ Y. Meir, N. S. Wingreen and P. A. Lee, *Phys. Rev. Lett.* **66**, 3048 (1991); Y. Meir and N. S. Wingreen, *Phys. Rev. Lett.* **68**, 2512 (1992).
¹² S. Sanvito, Chapter 7: Electron Transport Theory for Large Systems, in *Computational Nanoscience* (The Royal Society of Chemistry, 2011).
¹³ D. A. Ryndyk, R. Gutiérrez, B. Song, G. Cuniberti, in *Energy Flow Dynamics in Biomaterial Systems*, edited by E. Bittner, V. May, D. A. Micha, and I. Burghardt (Springer, Heidelberg, 2009).
¹⁴ A. R. Rocha, V. M. García-Suárez, S. Bailey, C. Lambert, J. Ferrer and S. Sanvito, *Phys. Rev. B* **73**, 085414 (2006).
¹⁵ I. Rungger and S. Sanvito, *Phys. Rev. B* **78**, 035407 (2008).
¹⁶ S. Kurth, G. Stefanucci, C.-O. Almbladh, A. Rubio, and E. K. U. Gross, *Phys. Rev. B* **72**, 035308 (2005).
¹⁷ P. Tröster, P. Schmitteckert and F. Evers, *Phys. Rev. B* **85**, 115409 (2012).
¹⁸ J. P. Bergfield, Z.-F. Liu and K. Burke and C. A. Stafford, *Phys. Rev. Lett.* **108**, 066801 (2012).
¹⁹ J. P. Perdew, R. G. Parr, M. Levy, and J. L. Balduz, Jr., *Phys. Rev. Lett.* **49**, 1691 (1982); J. P. Perdew and M. Levy, *Phys. Rev. Lett.* **51**, 1884 (1983).
²⁰ C. Toher, A. Filippetti, S. Sanvito and K. Burke, *Phys. Rev. Lett.* **95**, 146402 (2005).
²¹ C. Toher and S. Sanvito, *Phys. Rev. Lett.* **99**, 056801 (2007).
²² M. Koentopp, C. Chang, K. Burke and R. Car, *J. Phys.: Condens. Matter* **20**, 083203 (2008).
²³ G. Vignale and M. Di Ventra, *Phys. Rev. B* **79**, 14201 (2009).
²⁴ *Time-Dependent Density Functional Theory*, Lecture Notes in Physics, Vol. 706, edited by M. A. L. Marques, C. A. Ullrich, F. Nogueira, A. Rubio, K. Burke, and E. K. U. Gross (Springer, Berlin, 2006).
²⁵ M. Cini, *Phys. Rev. B* **22**, 5887 (1980).
²⁶ G. Stefanucci and C.-O. Almbladh, *Phys. Rev. B* **69**, 195318 (2004).
²⁷ S. Kurth, G. Stefanucci, E. Khosravi, C. Verdozzi, and E. K. U. Gross, *Phys. Rev. Lett.* **104**, 236801 (2010).
²⁸ E. J. McEniry, D. R. Bowler, D. Dundas, A. P. Horsfield, C. G. Sánchez and T. N. Todorov, *J. Phys.: Condens. Matter* **19**, 196201 (2007).
²⁹ T. N. Todorov, D. Dundas, and E. J. McEniry, *Phys. Rev. B* **81**, 075416 (2010).
³⁰ E. J. McEniry, T. N. Todorov and D. Dundas, *J. Phys.: Condens. Matter* **21**, 195304 (2009).
³¹ N. A. Lima, M. F. Silva, L. N. Oliveira and K. Capelle, *Phys. Rev. Lett.* **90**, 146402 (2003); K. Capelle, N. A. Lima, M. F. Silva and L. N. Oliveira, in *Progress in Theoretical Chemistry and Physics*, edited by N. I. Gi-

- dopoulos and S. Wilson (Kluwer, Dordrecht, 2003).
- ³² A. Nishino, T. Imamura, and N. Hatano, Phys. Rev. Lett. **102**, 146803 (2009); A. Nishino, T. Imamura, and N. Hatano, Phys. Rev. B **83**, 035306 (2011).
- ³³ B. Doyon, Phys. Rev. Lett. **99**, 076806 (2007).
- ³⁴ E. Boulat, H. Saleur, and P. Schmitteckert, Phys. Rev. Lett. **101**, 140601 (2008).
- ³⁵ I. Bâldea and H. Köppel, Phys. Rev. B **81**, 193401 (2010).
- ³⁶ G. Grüner and A. Zawadowski, Rep. Prog. Phys. **37**, 1497 (1974).
- ³⁷ O. Gunnarson and K. Schonhammer, Phys. Rev. Lett. **56**, 1968 (1986); K. Schonhammer, O. Gunnarson, and R. M. Novak, Phys. Rev. B **52**, 2504 (1995).
- ³⁸ A.-M. Uimonen, E. Khosravi, A. Stan, G. Stefanucci, S. Kurth, R. van Leeuwen, E. K. U. Gross. Phys. Rev. B **84**, 115103 (2011)
- ³⁹ E. Khosravi, A.-M. Uimonen, A. Stan, G. Stefanucci, S. Kurth, R. van Leeuwen and E. K. U. Gross, Phys. Rev. B **85**, 075103 (2012).
- ⁴⁰ J. Thijssen, *Computational Physics* (Cambridge University Press, 2007), p. 473.
- ⁴¹ T. N. Todorov, J. Phys.: Condens. Matter **14**, 3049 (2002).
- ⁴² R. Hanson, L. P. Kouwenhoven, J. R. Petta, S. Tarucha and L. M. K. Vandersypen, Rev. Mod. Phys. **79**, 1217 (2007).
- ⁴³ H. Bruus and K. Flensberg, *Many-Body Quantum Theory in Condensed Matter Physics: An Introduction* (Oxford University Press, 2007), p. 166.
- ⁴⁴ A. Akande and S. Sanvito, Phys. Rev. B **82**, 245114 (2010).
- ⁴⁵ We have established that if $|\gamma_0|$ is increased from 1 eV to 3.88 eV, the result for the current, obtained using two limits for the on-site energies of the leads, differ by at most 3% for $V_{sd}=4$ eV and for V_g between 0 and 1 eV.